Electronic Supplementary Material (ESI) for Dalton Transactions.

Yb^{3+} can be much better than Dy^{3+}: SMM properties and controllable self-assembly of novel lanthanide 3,5-dinitrobezoate-acetylacetonate complexes

Andrey V. Gavrikov[a,*], Nikolay N. Efimov[a,*], Andrey B. Ilyukhin[a],
Zhanna V. Dobrokhotova[a] and Vladimir M. Novotortsev[a]

[a] *N.S. Kurnakov Institute of General and Inorganic Chemistry, Russian Academy of Sciences, Leninsky prosp. 31, 119991 Moscow, Russian Federation. E-mail: penguin1990@yandex.ru (AVG), nnefimov@narod.ru (NNE)*

Contents

Table S1. Crystal data and structure refinement for **1-8**.

Identification code	**1**	**2**	**3**
Empirical formula	$C_{38}H_{50}Eu_2N_4O_{24}$	$C_{38}H_{50}Gd_2N_4O_{24}$	$C_{38}H_{50}N_4O_{24}Tb_2$
Formula weight	1250.76	1261.33	1264.68
Temperature, K	298	298	298
Wavelength, Å	1.5419	1.5419	1.5419
Crystal system	Triclinic	Triclinic	Triclinic
Space group	P-1	P-1	P-1
a, Å	8.3344(11)	8.3192(10)	8.3005(9)
b, Å	12.2094(10)	12.2662(9)	12.2891(11)
c, Å	13.4616(8)	13.4777(6)	13.4687(9)
α, °	68.853(7)	68.626(6)	68.471(9)
β, °	88.756(11)	88.583(9)	88.531(9)
γ, °	74.108(8)	74.046(7)	73.972(6
Volume, Å^3	1224.2(2)	1227.03(19)	1223.9(2)
Z	1	1	1

Identification code	**4**	**5**	**6**	**7**	**8**
Empirical formula	$C_{38}H_{50}Dy_2N_4O_{24}$	$C_{38}H_{50}Ho_2N_4O_{24}$	$C_{38}H_{50}Er_2N_4O_{24}$	$C_{38}H_{50}N_4O_{24}Tm_2$	$C_{38}H_{50}N_4O_{24}Yb_2$
Formula weight	1271.82	1276.68	1281.34	1284.68	1292.90
Temperature, K	150(2)	150(2)	120(2)	150(2)	150(2)
Wavelength, Å	0.71073	0.71073	0.71073	0.71073	0.71073
Crystal system	Triclinic	Triclinic	Triclinic	Triclinic	Triclinic
Space group	P-1	P-1	P-1	P-1	P-1
a, Å	8.2404(14)	8.2284(4)	8.1860(3)	8.1770(4)	8.1618(4)
b, Å	12.026(2)	12.0412(5)	12.0866(5)	12.1187(6)	12.1248(7)
c, Å	13.259(2)	13.2437(6)	13.1847(5)	13.2254(6)	13.1973(7)
α, °	69.446(6)	69.4450(10)	69.4010(10)	69.2020(10)	69.077(2)
β, °	89.417(6)	89.3480(10)	89.6460(10)	89.3350(10)	89.278(2)
γ, °	74.285(6)	74.1940(10)	74.2250(10)	74.1100(10)	74.064(2)
Volume, Å^3	1179.1(3)	1177.01(9)	1169.30(8)	1173.00(10)	1167.69(11)

Z	1	1	1	1	1
D (calc), Mg/m^3	1.791	1.801	1.820	1.819	1.839
μ, mm^{-1}	3.234	3.426	3.654	3.847	4.070
F(000)	630	632	634	636	638
Crystal size, mm	0.35 x 0.02 x 0.02	0.3 x 0.08 x 0.04	0.2 x 0.12 x 0.04	0.24 x 0.1 x 0.08	0.32 x 0.08 x 0.04
θ range, °	2.579, 26.324	2.584, 32.051	2.598, 30.113	2.602, 33.163	2.607, 29.215
Index ranges	-10<=h<=10	-12<=h<=11	-11<=h<=11	-12<=h<=12	-11<=h<=11
	-14<=k<=14	-17<=k<=17	-17<=k<=16	-18<=k<=18	-16<=k<=16
	-16<=l<=13	-19<=l<=18	-18<=l<=18	-20<=l<=20	-17<=l<=18
Reflections collected	9572	16878	16381	31341	15398
Independent reflections, Rint	4726, 0.0576	7308, 0.0352	6832, 0.0396	8546, 0.0280	6300, 0.0352
Completeness to θ = 25.242°	99.8 %	99.9 %	99.9 %	99.9 %	99.9 %
Absorption correction	Semi-empirical from equivalents	Semi-empirical from equivalents	Semi-empirical from equivalents	Semi-empirical from equivalents	Semi-empirical from equivalents
Max,. min. transmission	0.7454, 0.5481	0.7463, 0.5127	0.746, 0.573	0.7465, 0.5948	0.7458, 0.5283
Refinement method	Full-matrix least-squares on F^2	Full-matrix least-squares on F^2	Full-matrix least-squares on F^2	Full-matrix least-squares on F^2	Full-matrix least-squares on F^2
Data / restraints / parameters	4726 / 33 / 344	7308 / 9 / 327	6832 / 33 / 346	8546 / 9 / 327	6300 / 9 / 327
Goodness-of-fit	1.016	1.015	0.964	1.034	0.981
R1, wR2 [I>2sigma(I)]	0.0531, 0.0955	0.0316, 0.0658	0.0316, 0.0614	0.0230, 0.0509	0.0281, 0.0593
R1, wR2 (all data)	0.0872, 0.1068	0.0406, 0.0690	0.0460, 0.0656	0.0302, 0.0539	0.0372, 0.0627
Largest diff. peak and hole, $e.Å^{-3}$	2.229, -1.604	1.865, -1.061	1.218, -1.006	1.279, -0.556	1.623, -0.809

Table S2. Bond lengths Ln-O [Å] for **4-8**.

	Dy (**4**)	Ho (**5**)	Er (**6**)	Tm (**7**)	Yb (**8**)
Ln(1)-O(1)	2.334(5)	2.324(2)	2.318(2)	2.3065(14)	2.290(2)
Ln(1)-O(2)#1	2.337(5)	2.325(2)	2.312(2)	2.3057(14)	2.287(2)
Ln(1)-O(7)	2.354(5)	2.3473(19)	2.337(2)	2.3281(14)	2.315(2)
Ln(1)-O(8)	2.296(5)	2.282(2)	2.275(2)	2.2634(15)	2.250(2)
Ln(1)-O(9)	2.362(5)	2.363(2)	2.350(2)	2.3409(14)	2.333(2)
Ln(1)-O(10)	2.290(6)	2.283(2)	2.269(2)	2.2565(15)	2.243(2)
Ln(1)-O(11)	2.443(5)	2.433(2)	2.419(2)	2.4196(14)	2.403(2)
Ln(1)-O(12)	2.452(5)	2.454(2)	2.444(2)	2.4376(15)	2.429(2)
Ln(1)…Ln(1)#1	5.1490(10)	5.1362(3)	5.1291(3)	5.1171(2)	5.1081(3)

Symmetry transformations used to generate equivalent atoms:

#1 -x,-y,-z+1

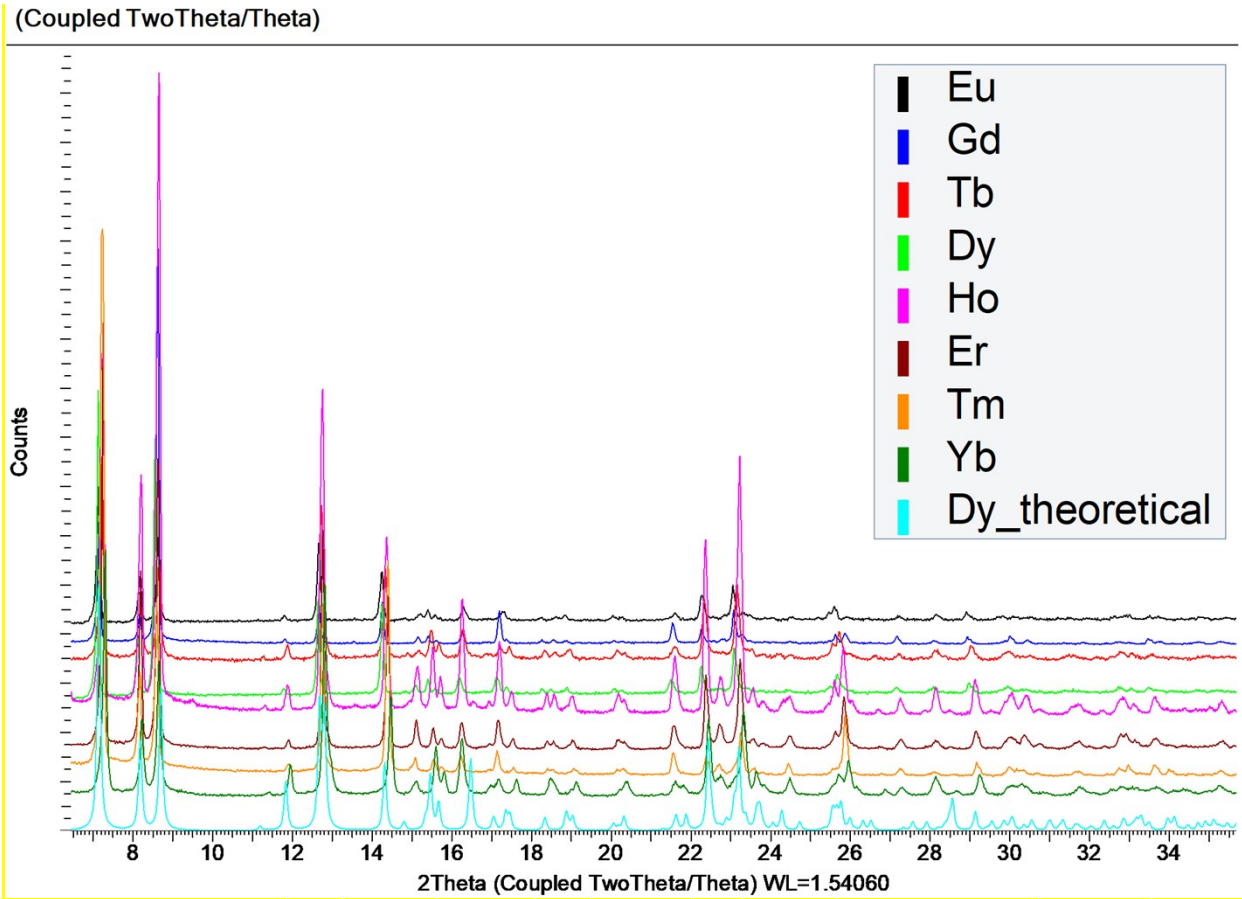

Fig.S1. Experimental (Eu (**1**),Gd (**2**), Tb (**3**), Dy (**4**), Ho (**5**), Er (**6**), Tm (**7**),Yb (**8**)) and theoretical (Dy) powder X-ray diffraction patterns of complexes under study.

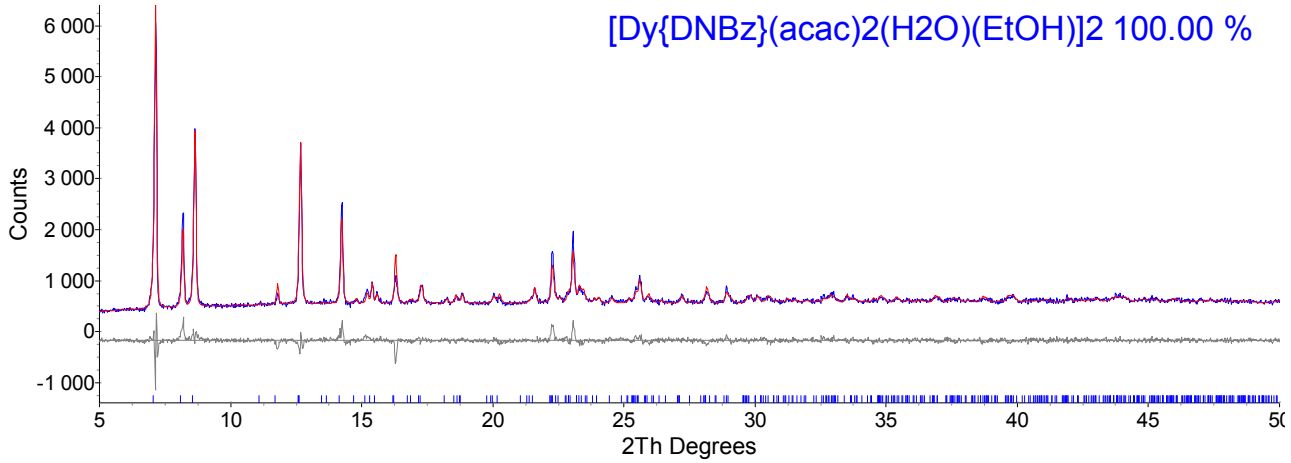

a

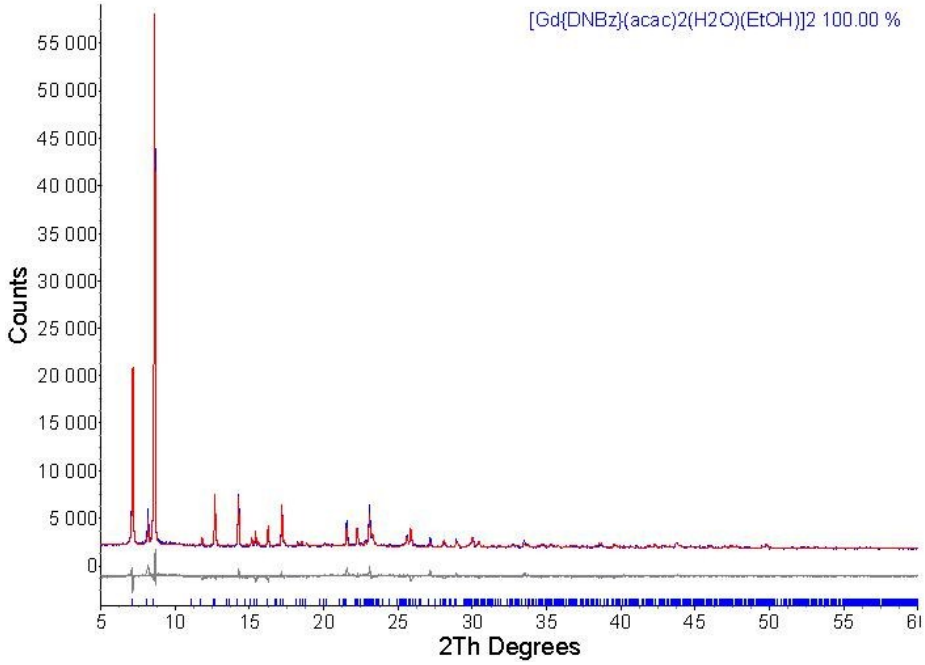

b

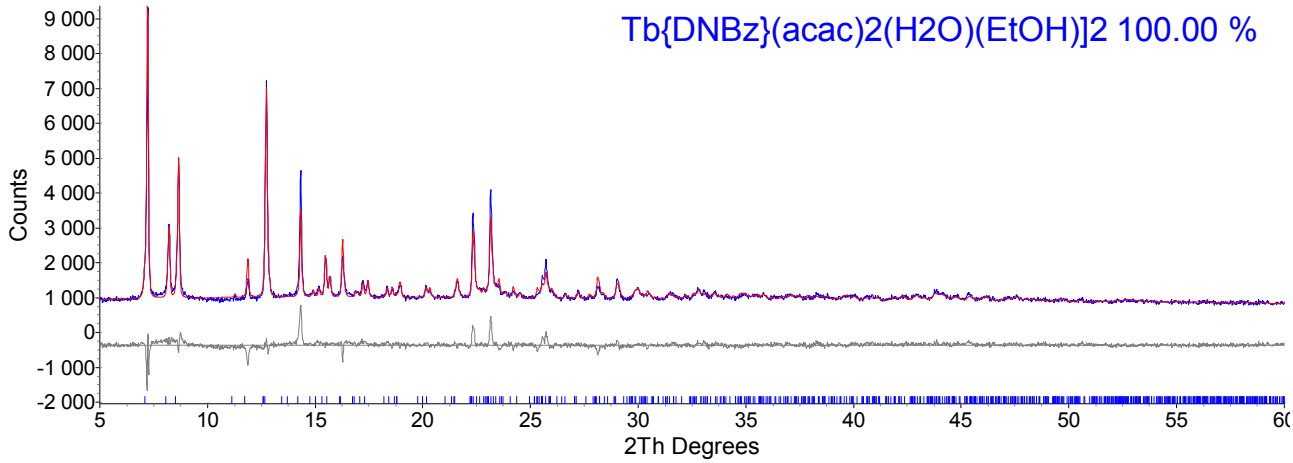

c

Fig.S2. Rietveld refinement profiles for (a) **1**, (b) **2**, and (c) **3** for room temperature X-ray data. The calculated and experimental profiles are shown with the red and blue line, respectively. The bottom trace shows the difference curve. The vertical bars indicate the calculated positions of the Bragg peaks.

Table S3. Shape consideration of the coordination polyhedron for complexes **4-8**.

S H A P E v2.1 Continuous Shape Measures calculation

(c) 2013 Electronic Structure Group, Universitat de Barcelona

Contact: llunell@ub.edu

Gavrikov6

SAPR-8	5 D4d Square antiprism
TDD-8	6 D2d Triangular dodecahedron
JBTPR-8	9 C2v Biaugmented trigonal prism J50
BTPR-8	10 C2v Biaugmented trigonal prism

Structure [ML8]	**SAPR-8**	**TDD-8**	**JBTPR-8**	**BTPR-8**
Dy	0.616	1.435	1.483	1.184
Ho	0.619	1.411	1.469	1.190
Er	0.603	1.431	1.470	1.178
Tm	0.599	1.408	1.439	1.171
Yb	0.631	1.365	1.427	1.174

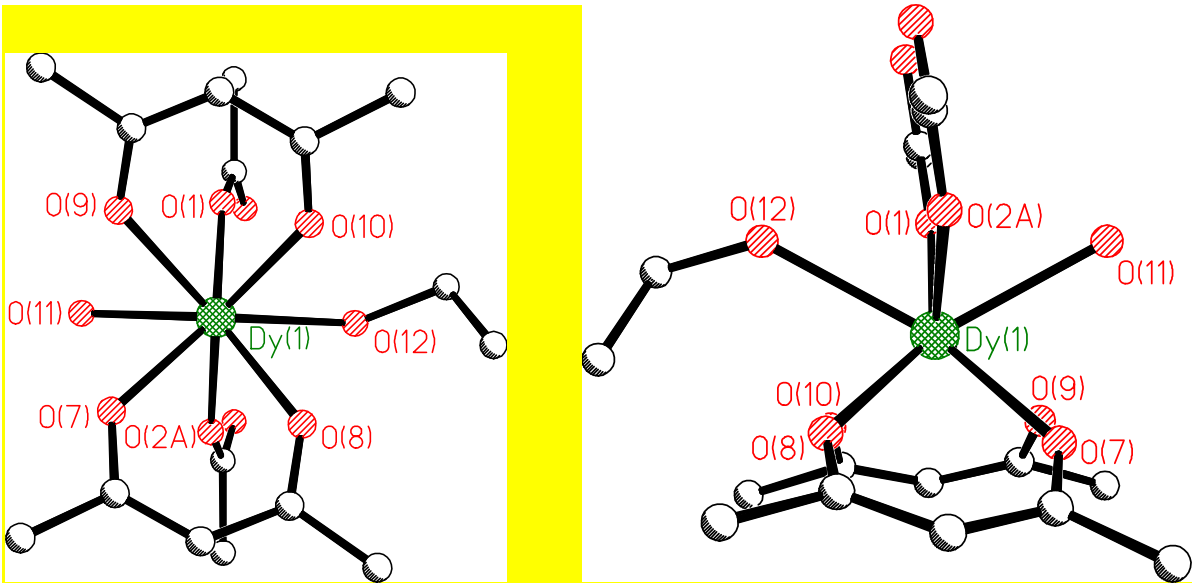

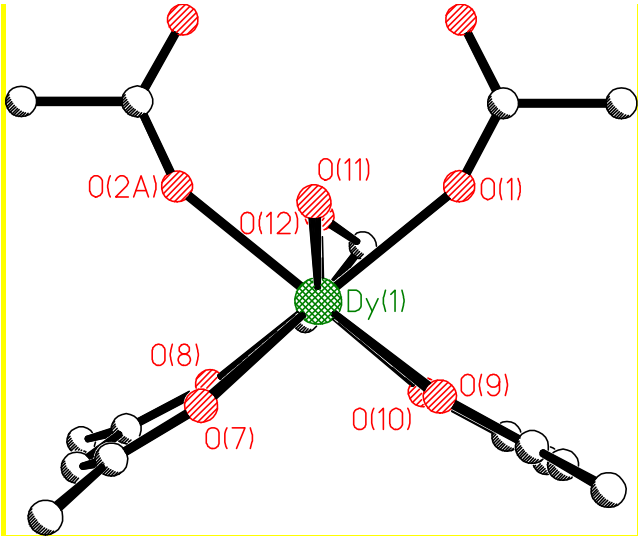

Plane	Mean deviation from plane
O(1)O(2A)O(11)O(12)	0.151
O(7)O(8)O(9)O(10)	0.054
O(1)O(2A)O(8)O(10)	0.024
O(1)O(2A)O(7)O(9)	0.028

IR study of 1-8

Complete and correct assignment of bands in the IR spectra of **1-8** is extremely difficult, since many of these bands are obviously overlapped with the bands of the initial compounds, i.e. $Ln(acac)_3 \cdot 3H_2O$ and Hdnbz. Nevertheless, a comparative study of the IR spectra of compounds **1-8** and initial reagents made it possible to reveal informative regions (Fig. S2) the analysis of which allows one to evidence the formation of complexes **1-8** reliably.

A comparative study of IR spectra in the region of 740-670 cm^{-1} revealed two bands for **1-8**, which correspond to the deformation vibrations of the $dnbz^-$ aromatic ring and of the $-NO_2$ groups of $dnbz^-$ [30]. E.g., for **1**, these bands are at 726 and 708 cm^{-1}, respectively (Fig. S2a) and are noticeably shifted to the higher frequencies range in comparison with those in the spectrum of Hdnbz (717 and 694 cm^{-1}, respectively). In the IR spectra of $Ln(acac)_3 \cdot 3H_2O$, there are no bands in this region. The formation of **1-8** is also confirmed *via* comparative analysis of IR spectra in the 2850-3100 cm^{-1} range, i.e. of the C-H valence vibrations, ν(CH). For **1-8**, there are C-H valence vibrations of both core-forming ligands, i.e. $C(sp^3)$-H ($acac^-$) and $C(sp^2)$-H (dnbz-) in this region (Fig. S2b). At the same time, in the IR spectrum of Hdnbz, there are obviously only $C(sp^2)$-H bands [30]. The presence of very weak band in the region of 3100-3000 cm^{-1} in $Ln(acac)_3 \cdot 3H_2O$ is due to the presence of $C(sp^2)$-H bonds with the C atom involved in the chelate cycles.

Thus, in spite of the inability to provide the correct assignment of the bands in the most characteristic regions of IR spectra of **1-8** (i.e., in the range of stretching vibrations of COO^- groups), IR spectroscopy can still be applied as a reliable method for preliminary identification of heteroleptic complexes formed in the $Ln(acac)_3$-RCOOH-Ligands/Solvents systems.

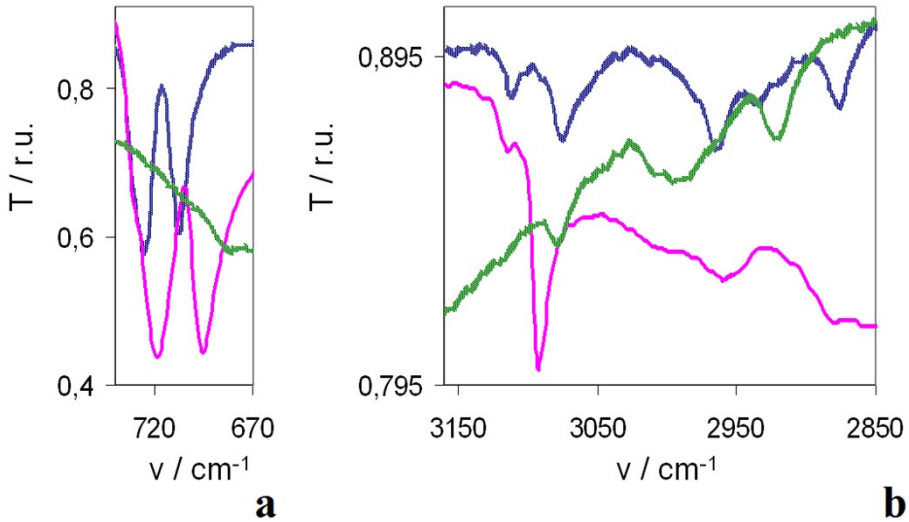

Fig. S3. IR spectra of compound **1** (blue line) in comparison with IR spectra of Hdnbz (pink line) and $Eu(acac)_3 \cdot 3H_2O$ (green line), in the range of 740-670 cm^{-1} (**a**) and 3160-2850 cm^{-1} (**b**).

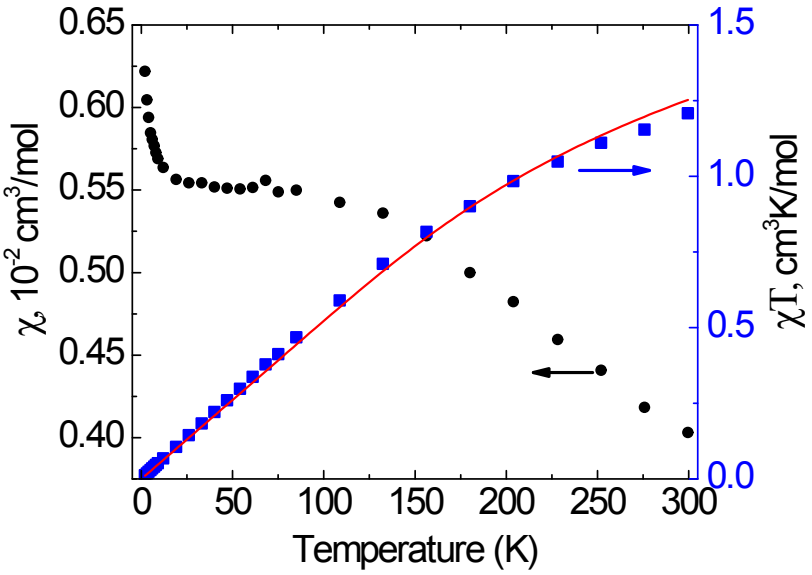

Fig. S4. $\chi_m T$ *vs.* T dependence per Eu^{3+} ion for complex **1** Eu at 5000 Oe. Solid line is approximation with the theoretical curve.

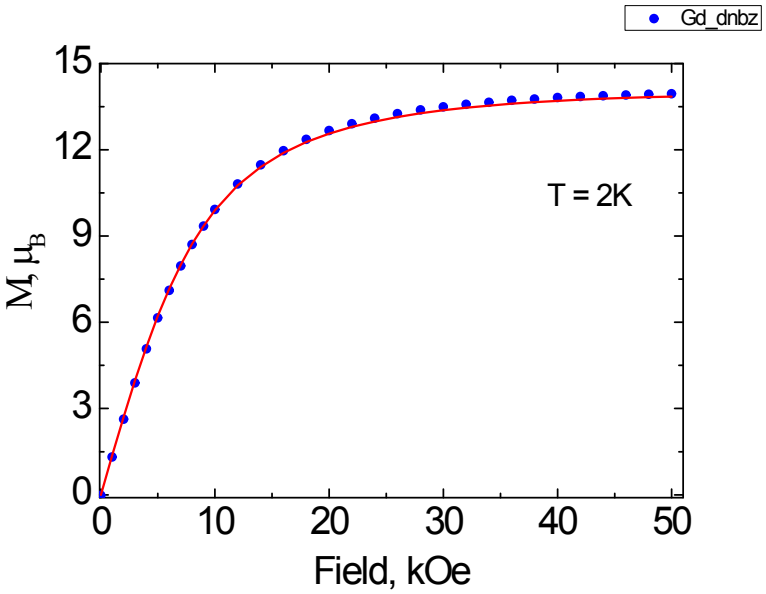

Fig. S5. Field dependence of the magnetization for Gd based complex **2** at 2 K. Red line represents the approximation with the theoretical curve with parameters described in the text.

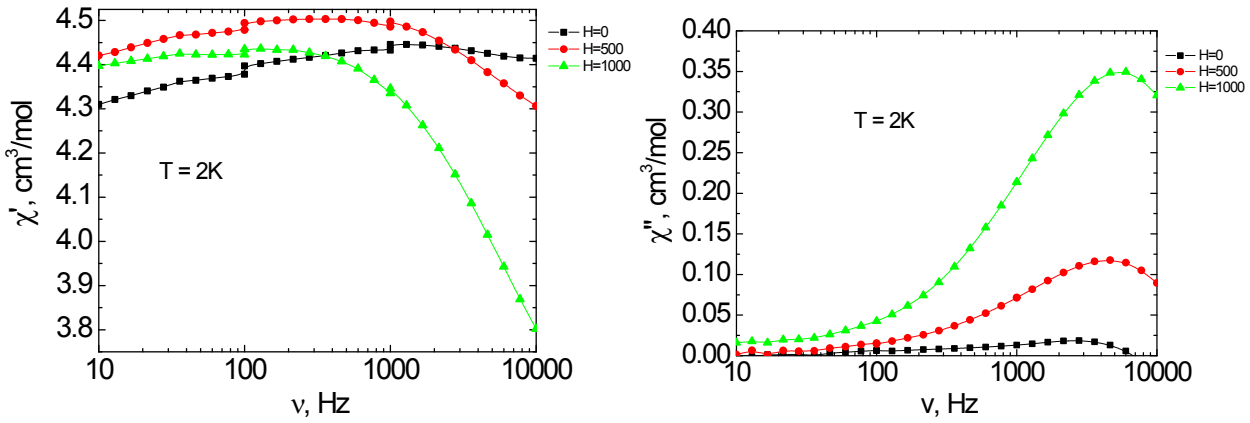

Fig. S6. Frequency dependence of χ' (left) and χ" (right) for a polycrystalline sample of **3** (Tb) at 2 K under 0-1000 Oe (step 500 Oe) *dc* fields.

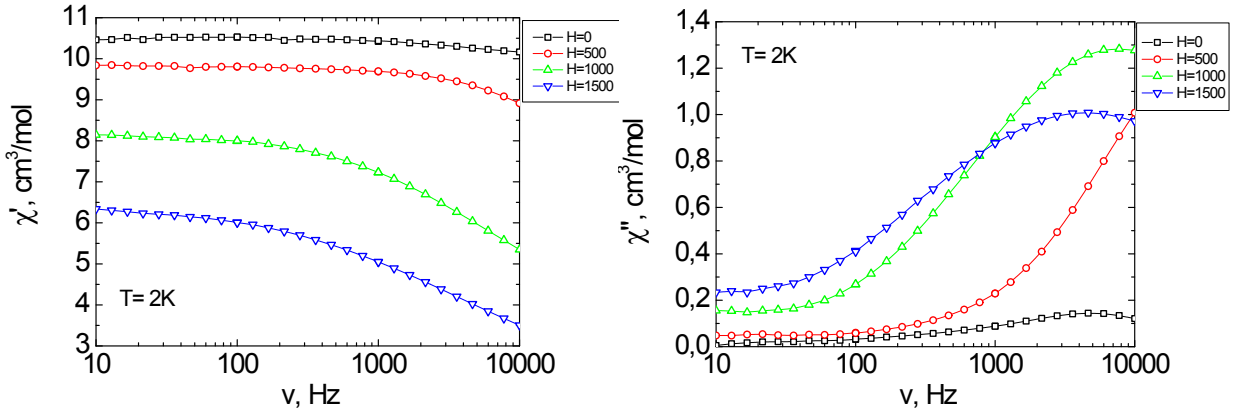

Fig. S7. Frequency dependence of χ' (left) and χ" (right) for a polycrystalline sample of **4** (Dy) at 2 K under 0-1500 Oe (step 500 Oe) *dc* fields.

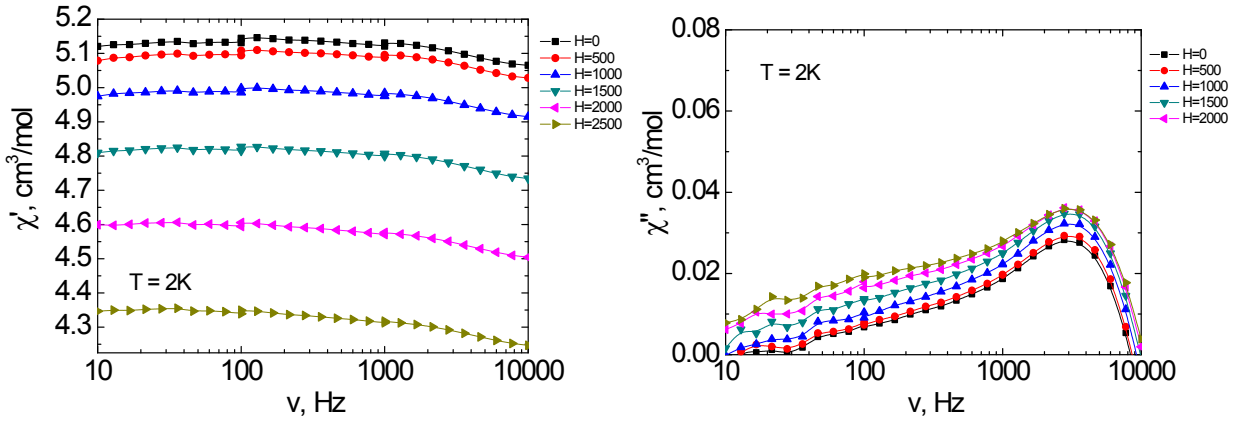

Fig. S8. Frequency dependence of χ' (left) and χ" (right) for a polycrystalline sample of **5** (Ho) at 2 K under 0-2000 Oe (step 500 Oe) *dc* fields.

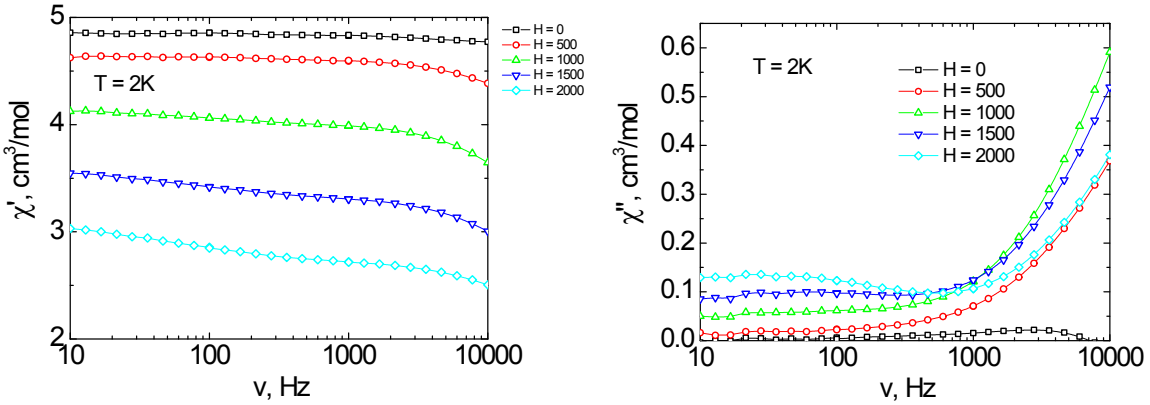

Fig. S9. Frequency dependence of χ' (left) and χ'' (right) for a polycrystalline sample of **6** (Er) at 2 K under 0-2000 Oe (step 500 Oe) *dc* fields.

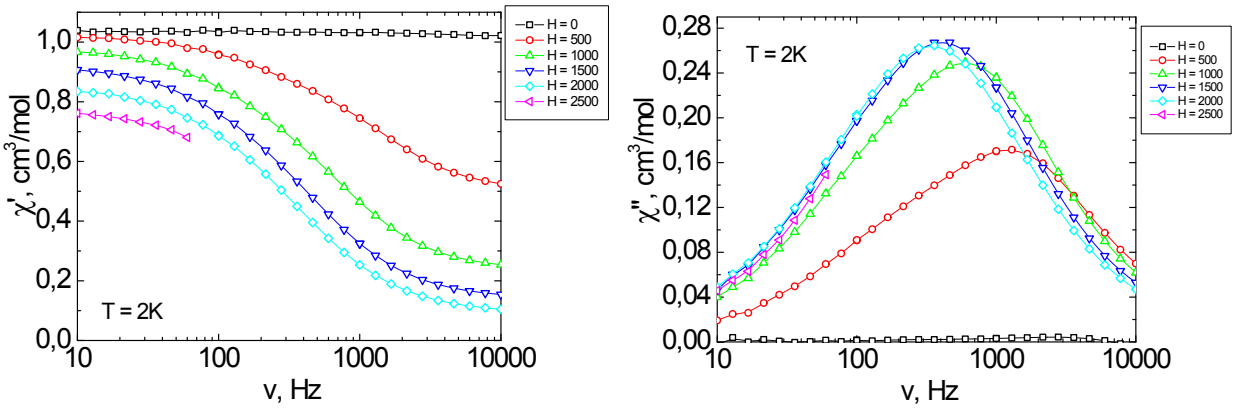

Fig. S10. Frequency dependence of χ' (left) and χ'' (right) for a polycrystalline sample of **8** (Yb) at 2 K under 0-2500 Oe (step 500 Oe) *dc* fields.

Shape measures calculation and structural discussion for the complexes given in Table 2 of the Main Text.

S H A P E v2.1 Continuous Shape Measures calculation
(c) 2013 Electronic Structure Group, Universitat de Barcelona
Contact: llunell@ub.edu

JCSAPR-9	7 C4v Capped square antiprism J10
CSAPR-9	8 C4v Spherical capped square antiprism
JTCTPR-9	9 D3h Tricapped trigonal prism J51
TCTPR-9	10 D3h Spherical tricapped trigonal prism
MFF-9	13 Cs Muffin

Structure [ML9]	JCSAPR-9	CSAPR-9	JTCTPR-9	TCTPR-9	MFF-9
$[Yb(DOTA)(H_2O)]^-$	1.069	0.463	2.773	1.346	1.183

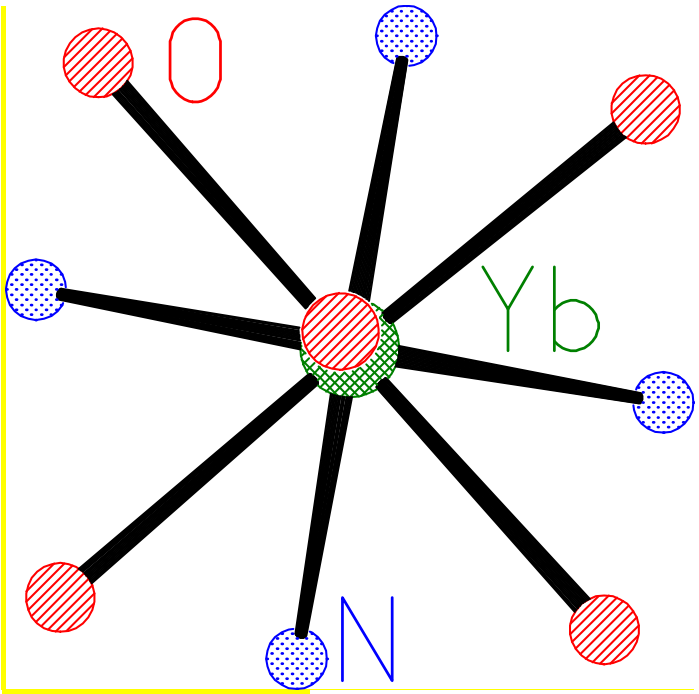

$[Yb(DOTA)(H_2O)]^-$ in $Na[Yb(DOTA)(H_2O)]\cdot 4H_2O$

SAPR-8	5 D4d Square antiprism
TDD-8	6 D2d Triangular dodecahedron
JBTPR-8	9 C2v Biaugmented trigonal prism J50
BTPR-8	10 C2v Biaugmented trigonal prism
JSD-8	11 D2d Snub diphenoid J84

Structure [ML8]	SAPR-8	TDD-8	JBTPR-8	BTPR-8	JSD-8
$[Yb(dnbz)(acac)_2(H_2O)(EtOH)]_2$	0.631	1.365	1.427	1.174	3.349
$[Yb(acac)_2(PyrCOO^2)(H_2O)_2]$	0.701	1.353	2.304	1.743	3.488
$[Yb(tta^4)_2(L_I^5)(L_{II}^6)]_2 \cdot 1.4(CH_2Cl_2)$	3.894	1.512	2.939	2.640	2.368
$[Yb(\mu^3\text{-}OH)(na^8)(PyrCOO)]_n$	2.437	0.909	2.055	1.878	2.770
$\{[Yb(L^9)(H_2O)_3(DMF)]\cdot(HL)\cdot(H_2O)\}_n$	0.454	2.145	2.377	1.896	4.686

In the structure of **$[Yb(acac)_2(PyrCOO^2)(H_2O)_2]$**, mean deviation from the rms plane of one of square faces in square antiprismatic polyhedron is 0.124 Å. Whereas if to consider the Yb polyhedron as biaugmented trigonal prism, then its three rectangular faces are coplanar up to 0.022, 0.059, 0.071 Å. Thus, we can conclude that Yb atom in **$[Yb(acac)_2(PyrCOO^2)(H_2O)_2]$** is better to be described as in the biaugmented trigonal prismatic environment.
In the structure of **$\{[Yb(L^9)(H_2O)_3(DMF)]\cdot(HL)\cdot(H_2O)\}_n$**, mean deviation from the rms planes of the square faces in the square antiprismatic polyhedron are 0.037 and 0.083 Å. Thus, Yb polyhedron in this compound is better to be considered as square antiprism.

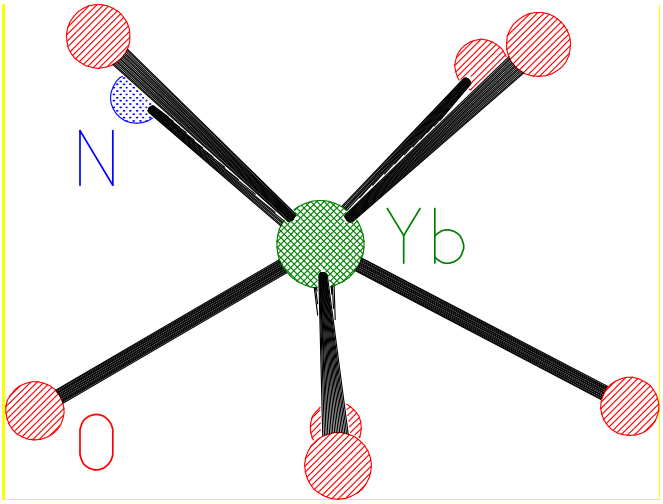

$[Yb(acac)_2(PyrCOO^2)(H_2O)_2]$

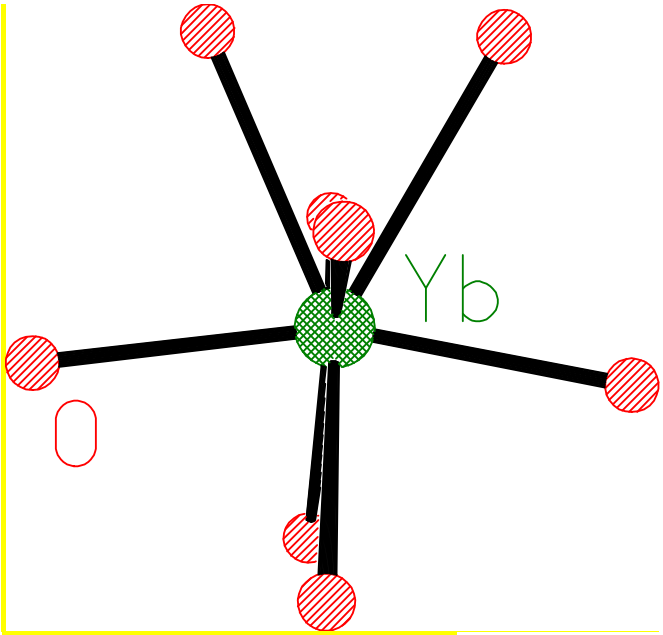

[Yb(tta[4])$_2$(L$_I$[5])(L$_{II}$[6])]$_2$·1.4(CH_2Cl_2)

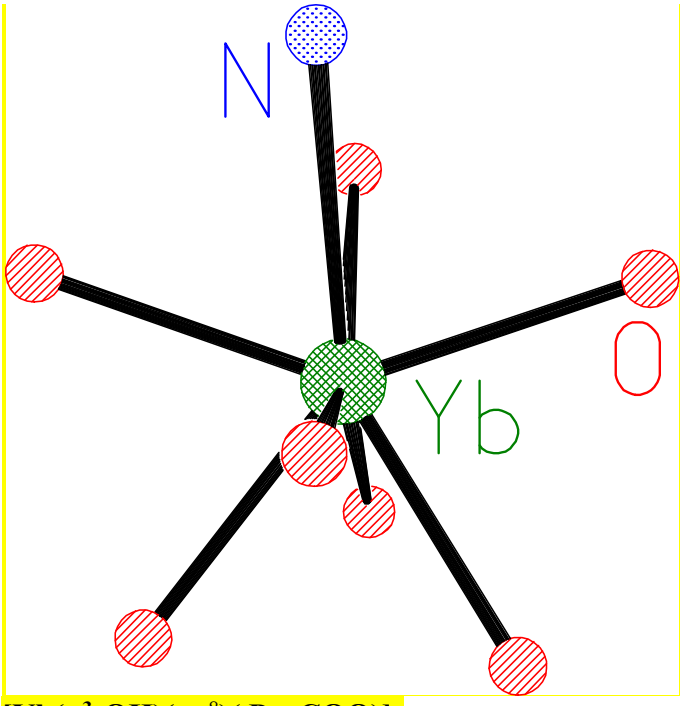

[Yb(μ[3]-OH)(na[8])(PyrCOO)]$_n$

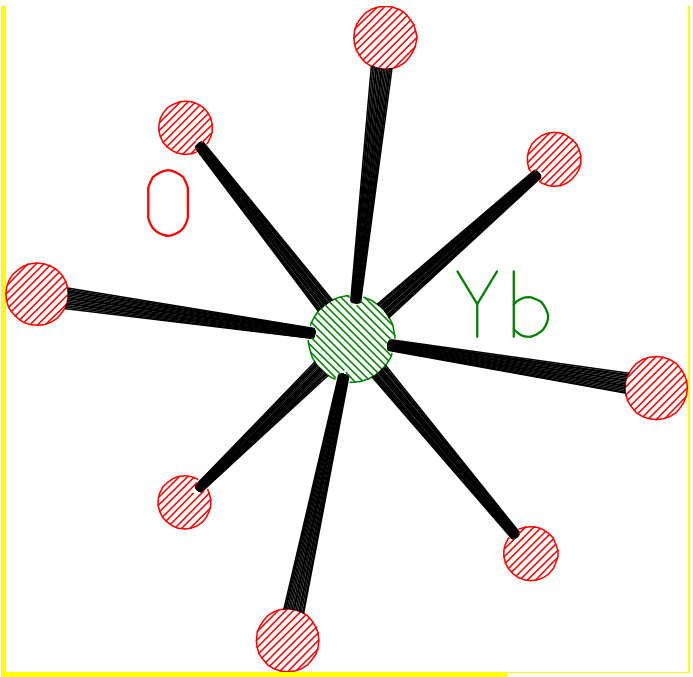

{[Yb(L^{9})(H$_2$O)$_3$(DMF)]·(HL)·(H$_2$O)}$_n$

PBPY-7	3 D5h Pentagonal bipyramid
COC-7	4 C3v Capped octahedron
CTPR-7	5 C2v Capped trigonal prism
JPBPY-7	6 D5h Johnson pentagonal bipyramid J13

Structure [ML7]	PBPY-7	COC-7	CTPR-7	JPBPY-7
[Yb(acac)$_2$(BcrCOO^{11})(H$_2$O)]$_n$	0.342	6.080	4.276	3.499

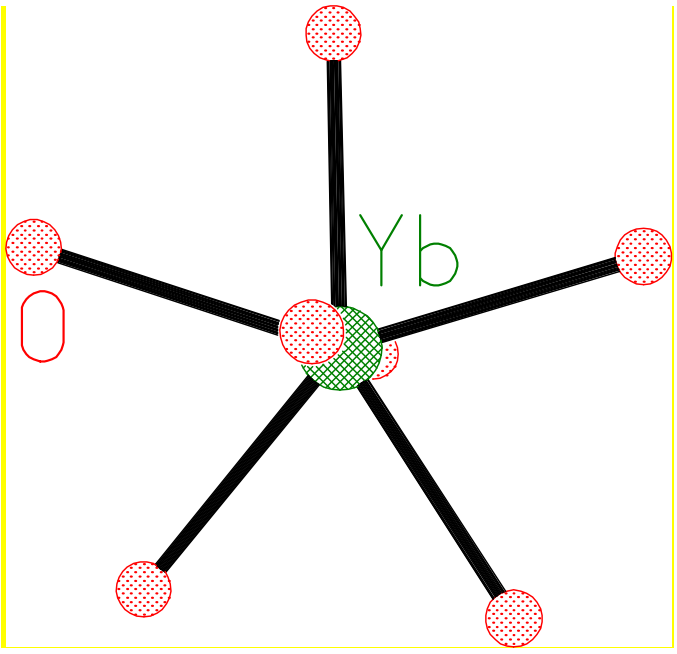

[Yb(acac)$_2$(BcrCOO^{11})(H$_2$O)]$_n$